Optik 127 (2016) 10102–10107

Contents lists available at ScienceDirect

Optik

journal homepage: www.elsevier.de/ijleo

Original research article

Structural investigations through cobalt effect on ZnO nanostructures

Y. Al-Douri[a,*], A.J. Haider[b], A.H. Reshak[c,d], A. Bouhemadou[e], M. Ameri[f]

[a] Institute of Nano Electronic Engineering, University Malaysia Perlis, 01000 Kangar, Perlis, Malaysia
[b] Nanotechnology and Advance Materials Research Center, University of Technology, 10066-Baghdad, Iraq
[c] New Technologies – Research Center, University of West Bohemia, Univerzitni 8, 306 14 Pilsen, Czech Republic
[d] Center of Excellence Geopolymer and Green Technology, School of Material Engineering, University Malaysia Perlis, 01007 Kangar, Perlis, Malaysia
[e] Laboratory for Developing New Materials and their Characterization, Department of Physics, Faculty of Science, University of Setif, 19000 Setif, Algeria
[f] Laboratory physico-chemistry of advanced materials, University of Djillali Liabes, BP 89, Sidi-Bel-Abbes, 22000, Algeria

ARTICLE INFO

Article history:
Received 7 June 2016
Accepted 8 August 2016

Keywords:
ZnO
Nanostructures
SEM
XRD

ABSTRACT

Co-doped ZnO nanostructures synthesized on glass substrate have been prepared using Pulsed Laser Deposition (PLD) technique. Scanning Electron Microscopy (SEM) and X-Ray diffraction (XRD) have utilized for characterization and analysis. The structural properties of lattice constants and bulk moduli are measured and calculated using specific model, respectively. The grain size, strain, stress and texture coefficient are investigated. The nano grain size is verified by SEM. The calculated results show good agreement with the experimental and theoretical data.

1. Introduction

Zinc oxide (ZnO) shows a large direct band gap (3.37 eV) and exciton binding energy (60 meV) as well as excellent chemical and thermal stability that may lead to important applications for ultraviolet devices, catalysis, piezoelectrics and gas sensors [1–5]. Different deposition techniques are used to fabricate ZnO nanostructures including electrochemical deposition technique [6], thermal oxidation [7], r.f. magnetron sputtering [8] and chemical bath deposition (CBD) [9]. Pulsed Laser Deposition (PLD) offers many advantages compared with other techniques; reduced contamination due to using laser light and control of composition of the deposited structure [10].

Recently, Zhang et al. [11] have deposited ZnO nanosheet on indium tin oxide (ITO)-coated glass substrates by galvanic displacement deposition process. This is to avoid high temperature and electric power to let it simple and cost-effective. The ZnO nanosheet has uniform wurtzite structure. The photoelectrochemical (PEC) cell based on ZnO nanosheet film/ITO photoelectrode was fabricated to improve its performance using optimized solution concentration. A higher photocurrent density of $\sim$500 μA cm^{-2} under AM 1.5 G simulated illumination of 100 mW cm^{-2} with zero bias potential (vs. Ag/AgCl electrode) was obtained that ascribed to increased surface-to-volume ratio of disordered ZnO nanosheet arrays. While, Li et al. [12] have prepared porous Zn–Sn–O nanocubes with a uniform size through a facile aqueous solution route combined with subsequent thermal treatment. The chemical composition, morphology, and microstructure of Zn–Sn–O nanocubes, which

* Corresponding author.
E-mail address: yaldouri@yahoo.com (Y. Al-Douri).

http://dx.doi.org/10.1016/j.ijleo.2016.08.012
0030-4026/

have significant effects on the lithium storage performances, were easily tuned by adjusting the calcination temperature in preparation processes of $ZnSn(OH)_6$ solid nanocubes. They have revealed that porous Zn–Sn–O nanocubes exhibits good rate capability and high reversible capacity of 700 mAh g^{-1} at a current density of 200 mA g^{-1} after 50 cycles that was great potential as anode materials in Lithium-ion batteries. Moreover, Augustine et al. [13] have tested the chemical and biological phenomena by using surface acoustic wave (SAW) device, that was fabricated by electrospinning poly(vinylidenefluoride-*co*-trifluoroethylene) (P(VDF–TrFE)) incorporated with zinc oxide (ZnO) nanoparticles. They have investigated the morphology, composition, and crystallinity of P(VDF–TrFE)/ZnO nanocomposites. It was found that insertion loss of the SAW devices incorporated with ZnO nanoparticles was much less than the neat polymer-deposited device. The mentioned device was utilized in acoustic biosensors to detect and quantify the cell proliferation in cell culture systems.

In this work, Co-doped ZnO nanostructures on glass substrates synthesized by Pulsed Laser Deposition (PLD) at 400 °C are prepared. We also investigated the influence of laser 0.4 J/cm^2 applied during the deposition process on the morphology, structural and hardness properties using specific model of bulk modulus of Co-doped ZnO nanostructures with different Co concentrations.

2. Experimental

Pure ZnO powder with high purity (99.999%) (Sigma–Aldrich) and powders doped with different concentrations for Co were prepared. The prepared powders were pressed till 5 tons to form a target with 2.5 cm diameter and 0.4 cm thickness. The target should be dense and homogenous as can as possible to ensure good quality of the deposits. It was mounted in locally design vacuum chamber and ablated by a double frequency with Q-switched Nd:YAG pulsed laser operated at 532 nm, pulse duration of about 10 ns and 0.4 J/cm^2 energy density was focused on the target to generate plasma plume. Amorphous fused silica (from Alfa Aesar) was used as substrates and grown in oxygen environment with O_2 partial pressure of 10 Pa at substrate temperature of 400 °C. The deposited nanostructures were grown typically 10 min after cooling to room temperature.

The mentioned technique has been utilized to test the overall structures of lattice constants, identification of unknown materials, orientation of single crystals and polycrystals, defects, stresses, etc. In this work, X-ray diffractometer (XRD) (SHIMADZU, USA) and power diffraction system with Cu-Kα x-ray tube (λ = 1.54056 Å) were used. The XRD was performed between 2θ values of 30°–38°. The morphological features of the various nanostructures were investigated with Scanning Electron Microscopy (SEM) (JEOL JSM-6360, USA) equipped with an energy dispersive X-ray spectroscopy detector. In the emission mode of SEM, electrons fired from a filament (tungsten hairpin or LaB_6) were accelerated with a voltage in the range of 1–30 kV down the center of an electron-optical column consisting of two or three magnetic lenses. To obtain the nanostructure thickness, an optical interferometer method has been used. It is basing on light beam reflected from surface and substrate interference. He-Ne laser wavelength is 0.632 μm and the determined thickness is:

$$d = \frac{\Delta x}{x} \times \frac{\lambda}{2}. \quad (1)$$

where x is the fringe width, Δx is the distance between two fringes and λ is wavelength of laser light. The nanostructure thickness using the above equation is 200 nm.

3. Results and discussion

3.1. Characterization of Co-ZnO nanostructures

Typical SEM images of undoped ZnO and Co-doped ZnO nanostructures are synthesized on glass substrates with 400 °C using pulsed laser deposition technique, 0.4 J/cm^2 laser energy and 10 Pa Oxygen pressure. The surface is very smooth and the crystallites are very fine. No big particles can be found from SEM image. The grain size is approximately 34–67 nm. It is found that the Co doping concentration has a significant influence on ZnO nanostructure surface structure. The grain size increases gradually as the Co concentration increases.

Therefore, the grain size has been investigated by SEM for Co doping as listed in Table 1. The grains become densely unpacked near regularly. The SEM micrographs show the surface of ZnO nanostructures with various Co content as shown in Fig. 1. The Co-free ZnO displays hexagonal shaped with submicron size diameter. As can be seen from Fig. 1, the diameter of nanostructures decreases at Co (5%) concentration due to Co influences the nanostructure morphology.

Table 1
Measured grain size using SEM and integral breadth, shape factor, strain, stress and texture coefficient using XRD of undoped ZnO and Co-ZnO nanostructures for different concentrations.

Sample T = 400 °C	FWHM (deg)	Grain size using SEM (nm)	Integral Breadth β	Shape factor Φ	Strain δ (%)	Stress σ	Texture Coef. T_C (hkl)
ZnO-pure	0.254	44	0.190	1.33	9.167	−0.0808	1.68
ZnO:Co (1%)	0.138	50	0.203	0.67	9.167	−0.0808	1.39
ZnO:Co (3%)	0.120	67	0.200	0.60	9.212	−0.0812	1.41
ZnO:Co (5%)	0.156	34	0.207	0.75	9.258	−0.0816	1.32

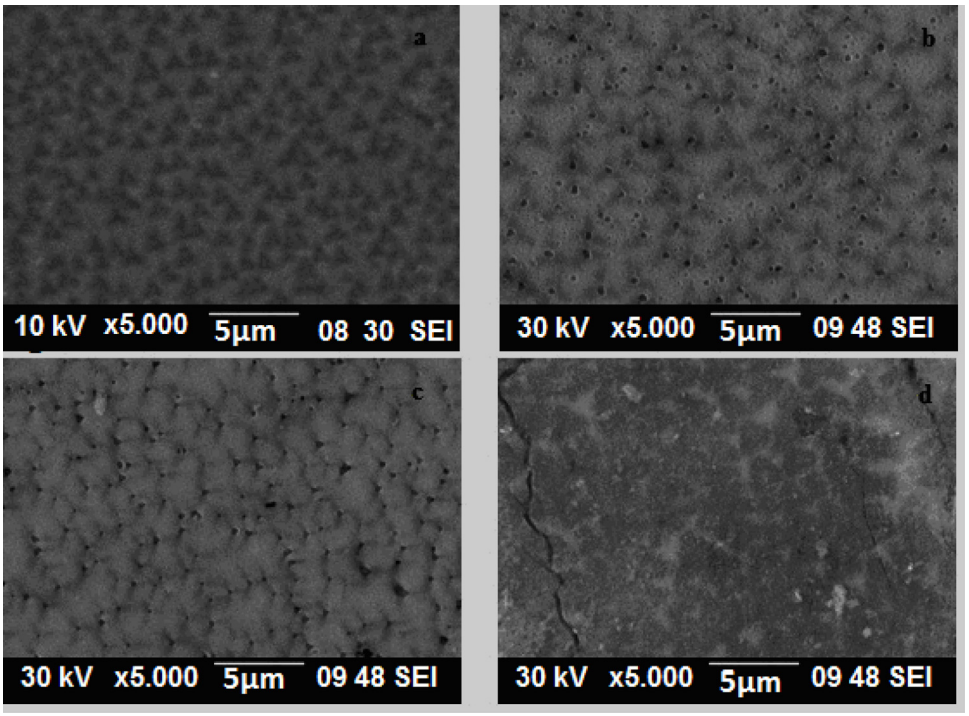

Fig. 1. SEM images of undoped ZnO (a) and Co-doped ZnO nanostructures for different concentrations (b) 1% Co, (c) 3% Co. and (d) 5% Co.

Table 2
Measured interplanar spacing, lattice constants and calculated bulk modulus of undoped ZnO and Co-ZnO nanostructures for different concentrations.

Sample	2θ (deg)	θ (deg)	d (Å)[a]	a (Å)[a]	c (Å)[a]	B_o[b] (GPa)
ZnO-pure T = 400 °C	31.748	15.87	2.813	3.248 3.249[d] 3.222[e]	5.300 5.204[d] 5.193[e]	196.26 166[f] 156.30[g] 183[h]
ZnO:Co (1%) T = 400 °C	31.74	15.87	2.813 1.99[c]	3.248	5.216	203.26
ZnO:Co (3%) T = 400 °C	31.76	15.88	2.814 1.99[c]	3.249	5.099	213.31
ZnO:Co (5%) T = 400 °C	31.75	15.87	2.815 1.98[c]	3.250	5.210	203.50

[a] Measured value.
[b] Calculated value using eq. (5).
[c] Ref. [17] Theor.
[d] Ref. [16] Exp.
[e] Ref. [16] Theor.
[f] Ref. [16] Theor.
[g] Ref. [35] Theor.
[h] Ref. [36] Exp.

3.2. Structural properties of Co-ZnO nanostructures

The XRD patterns of undoped ZnO and ZnO:Co nanostructures with different doping concentrations are shown in Fig. 2, the structure type is hexagonal with a strong (100) preferred orientation. No diffraction peaks of Co or other impurity phases are found in these samples. The angle of the dominant peak corresponding to (100) plane is at $2\theta = 31.7^{\circ}$ for the undoped ZnO film, and it changes as Co concentration increases. The intensity of XRD peaks is related to many factors, including crystallization quality, density and thickness of nanostructures. The intensities of ZnO (100) peaks in XRD patterns are different due to diverse crystallization quality and various substrate temperatures in spite of the same deposition condition [14]. The increasing of peak intensity indicates an improvement in the nanostructures crystallinity with increasing grain size [15].

One can see the deposition nanostructures display a hexagonal structure of ZnO. Significant changes observed in the XRD patterns manifest them in increasing of peak intensity to correspond crystal plane (100) and a decreasing in the peak intensity for other planes. The lattice constants and the relative intensity ratio to (100) in the diffraction pattern of undoped ZnO nanostructures deposited under various doping concentrations are given in Table 2. The measured lattice constants are found to be in good agreement with experimental [16] and theoretical data [16,17].

The measured (c) values are found to be decreased from 5.3 Å for undoped ZnO to 5.21 Å for Co (5%). The observed decreasing in the c parameter may arise from the possible introduction of Co ions into interstitial sites [18]. It is noticed that the intensities of the characteristic peaks increase with increasing Co concentration of 3%, however, some decrease in

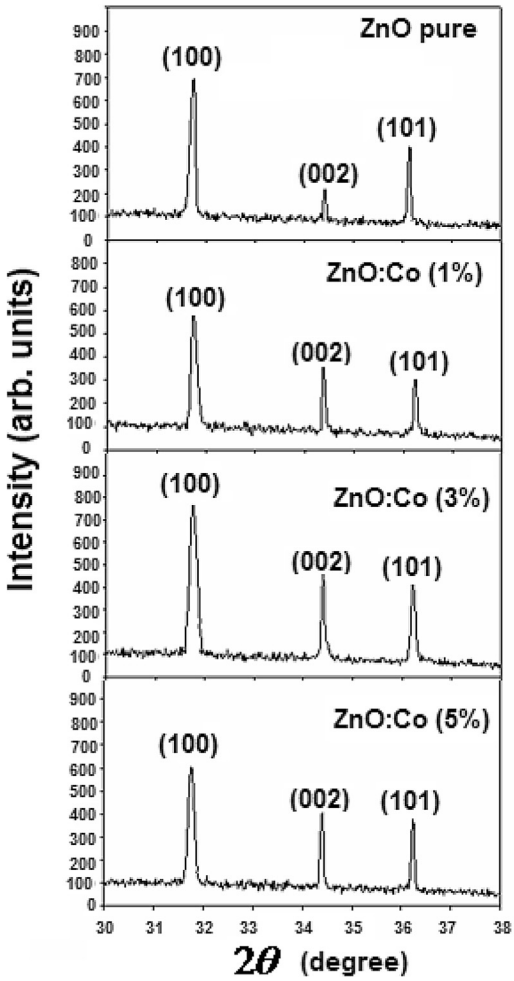

Fig. 2. XRD patterns of undoped ZnO (a) and Co-doped ZnO nanostructures for different concentrations (b) 1% Co, (c) 3% Co. and (d) 5% Co.

the intensities are observed for the Co concentration of about (1%) and (5%) as shown in Fig. 2. In addition, the interplanar spacing (d) is investigated and found to be in reasonable agreement with available results [17]. We should emphasize that d is directly proportional to the Co concentrations as given in Table 2.

The results of Full Width at Half Maximum (FWHM) for all samples point out that they have values close for undoped ZnO and ZnO:Co nanostructures of various doping concentrations. For Co concentrations (1%, 3% and 5%), the FWHM value is about (0.12°–0.15°) while for undoped ZnO, it is about 0.25° as given in Table 1.

The integral breadth (β) of the ZnO:Co nanostructures are obtained from XRD pattern sheets using [19,20]:

$$\beta = \frac{Area}{I_o} \tag{2}$$

where *Area* is the area under peak and I_o is the maximum intensity. Our results indicate that β increases with increasing of Co concentration as indicated in Table 1. Also, the shape factor (Φ) was calculated by [20,21];

$$\Phi = \frac{\Delta}{\beta} \tag{3}$$

The residual strain (δ) increases for all Co doping concentration. The stress (σ) is negative, so the biaxial stress is compressive [22]. Texture coefficient (Tc) of fabricated ZnO:Co nanostructures was calculated using [23]:

$$T_C(hkl) = \frac{[(I(hkl)/I_o(hkl)]}{[Nr - 1\sum I(hkl)/I_o(hkl)]} \tag{4}$$

where I is the measured intensity, I_o is the standard intensity, Nr is the reflection number and hkl is Miller indices. The results indicate that (Tc) decreases with increasing Co doping concentration and causes an increasing in the surface roughness as given in Table 1.

It is known that the bulk modulus is a reflectance of the materials hardness that it is important in different industries. Many authors [24–29] have made various efforts to explore thermodynamic properties of solids. In these studies, authors have examined the thermodynamic properties such as the inter-atomic separation and the bulk modulus of solids with different approximations and best-fit relations [26–29]. It has become possible to compute with great accuracy an important number of structural and electronic properties of solids. The *ab initio* calculations are complex and require significant effort. Therefore, more empirical approaches have been developed [30,31] to compute different properties for the materials. In many cases, the empirical methods offer the advantage of applicability to a broad class of materials and to illustrate trends. In many applications, these empirical approaches do not give highly accurate results for each specific material, but are still very useful. Cohen [32] had established an empirical formula for calculation of the bulk modulus B_0; based on the nearest-neighbor distance. His result is in agreement with experimental values. Lam et al. [33] had derived an analytical expression for the bulk modulus from the total energy. This expression is different in structure from the empirical formula but gives similar numerical results. In addition, they have obtained an analytical expression for the pressure derivative B_0 of the bulk modulus. Our group [34] had used a concept based on the lattice constant to establish an empirical formula for the calculation of the bulk modulus. The calculated results are in agreement with experimental data and other calculations. Consideration of hypothetical structure and simulation of the experimental conditions are required to make practical use of this formula.

The aim is to see how a qualitative concept, such as the bulk modulus, can be related to the lattice constant. It was argued that the dominant effect is the degree of covalency characterized by Phillips' homopolar gap E_h [30], and one reason for presenting these data here is that the validity of our calculations that is not restricted in computed space. Thus, we believe that the data will prove valuable future works in this field.

An important reason for studying B_0 is the observation of clear differences between the lattice constants for undoped and Co-doped ZnO nanostructures as given in Table 2. The basis of our model is the lattice constant as given in Table 2. Fitting of these data gives the following empirical formula [34]:

$$B_0 = [3000 - 100\lambda]\left(\frac{a}{2}\right)^{-3.5} \tag{5}$$

where a is the lattice constant (in Å) and λ is a constant equals 2 for group II–VI semiconductors. In Table 2, the calculated bulk moduli values are investigated and compared with the available theoretical results [16,35] and experimental data [36]. We may notice that the investigated bulk modulus of undoped ZnO is in accord with other results [16,35,36] and exhibits the same chemical trends as those found for Co-doped ZnO nanostructures as given in Table 2. Those investigated, theoretical and experimental results for ZnO:Co concentration are the same within the error by adding estimated error 7-10% after each calculated value of B_0. Our results show that ZnO:Co nanostructure at 3% is the hardest.

4. Conclusion

ZnO:Co nanostructures were synthesized on glass substrate by PLD at 400 °C and 10 Pa oxygen background gas. The structural properties are found to be dependent on the laser influence. The crystal structure of the nanostructures is hexagonal. The average grain size is investigated by SEM and found to be 34–67 nm. SEM indicates that the average grain size increases with increasing Co doping concentrations. It is concluded that the calculated bulk modulus for undoped and Co-doped ZnO nanostructures of different doping concentrations is the hardest at 3% in parallel with the bigger grain size of the same concentration.

Acknowledgments

Y. A. would like to acknowlegde University Malaysia Perlis for grant No. 9007-00185. For A.H.R., the result was developed within the CENTEM project, reg. no. CZ.1.05/2.1.00/03.0088, cofunded by the ERDF as part of the Ministry of Education, Youth and Sports OP RDI programme and, in the follow-up sustainability stage, supported through CENTEM PLUS (LO1402) by financial means from the Ministry of Education, Youth and Sports under the National Sustainability Programme I. Computational resources were provided by MetaCentrum (LM2010005) and CERIT-SC (CZ.1.05/3.2.00/08.0144) infrastructures.

References

[1] Z.W. Pan, Z.R. Dai, Z.L. Wang, Nanobelts of Semiconducting Oxides, Science 291 (2001) 1947.
[2] Z.R. Tian, J.A. Voigt, J. Liu, B. Mckenzie, M.J. Mcdermott, M.A. Rodriguez, H. Konishi, H. Xu, Complex and oriented ZnO nanostructures, Nat. Mater. 2 (2003) 821.
[3] B. Liu, H.C. Zeng, Fabrication of ZnO Dandelions via a Modified Kirkendall Process, J. Am. Chem. Soc. 126 (2004) 16744.
[4] M.H. Huang, S. Mao, H. Feick, H. Yan, Y. Wu, H. Kind, E. Weber, R. Russo, P. Yang, Room-temperature ultraviolet nanowire nanolasers, Science 292 (2001) 1897.
[5] Y.X. Wang, X. Ding, Y. Cheng, Y.J. Zhang, L.L. Yang, H.L. Liu, H.G. Fan, Y. Liu, J.H. Yang, Properties of Co-doped ZnO films prepared by electrochemical deposition, Cryst. Res. Technol. 44 (2009) 517.
[6] N.K. Hassan, M.R. Hashim, Y. Al-Douri, Morphology and optical investigations of ZnO pyramids and nanoflakes for optoelectronic applications, Optik 125 (2014) 2560.
[7] X.T. Zhang, Y.C. Liu, Z.Z. Zhi, J.Y. Zhang, Y.M. Lu, D.Z. Shen, W. Xu, X.W. Fan, X.G. Kong, Temperature dependence of excitonic luminescence from nanocrystalline ZnO films, J. Lumin. 99 (2002) 149.

[8] Q.P. Wang, X.J. Zhang, G.Q. Wang, S.H. Chen, X.H. Wu, H.L. Ma, Influence of excitation light wavelength on the photoluminescence properties for ZnO films prepared by magnetron sputtering, Appl. Surf. Sci. 254 (2008) 5100.
[9] Nguyen Thanh Son, Jin-Seo Noh, Sungho Park, Role of ZnO thin film in the vertically aligned growth of ZnO nanorods by chemical bath deposition, Appl. Surf. Sci. 379 (2016) 440.
[10] R. Eason, Pulsed laser Deposition of thin films Applications-led growth of functional Materials, John Wiley & Sons Inc., 2007.
[11] B. Zhang, F. Wang, C. Zhu, Q. Li, J. Song, M. Zheng, L. Ma, W. Shen, Nano-Micro Lett. 8 (2016) 137–142.
[12] B. Li, X. Li, J. Zai, X. Qian, Nano-Micro Lett. 8 (2016) 174–181.
[13] R. Augustine, F. Sarry, N. Kalarikkal, S. Thomas, L. Badie, D. Rouxel, Nano-Micro Lett. (2016), http://dx.doi.org/10.1007/s40820-016-0088-2.
[14] F.K. Shan, B.C. Shin, S.W. Jang, Y.S. Yu, Substrate effects of ZnO thin films prepared by PLD technique, J. Eur. Ceram. Soc. 24 (2004) 1015.
[15] P. Sagar, M. Kumar, R.M. Mehra, Electrical and optical properties of sol-gel derived ZnO:Al thin films, Mater. Sci. Pol. 23 (2005) 685.
[16] Y.Z. Zhu, G.D. Chen, H. Ye, A. Walsh, C.Y. Moon, S.-H. Wei, Electronic structure and phase stability of MgO, ZnO, CdO, and related ternary alloys, Phys. Rev. B 77 (2008) 245209.
[17] T.P. Yong, B.Sc dissertation, National University of Singapore, Singapore, 2006.
[18] D.R. Uhlmann, H.K. Bowen, W.D. Kingery, Introduction to Ceramics, John Wiley & Sons Inc, New York, 1976.
[19] C. Gümüs, O.M. Ozkendir, H. Kavak, Y. Ufuktepe, Structural studies of ZnO, J. Optoelectron. Adv. Mater. 8 (2006) 299.
[20] P. Šutta, Q. Jackuliak, Elastic constants of ZnO compound, Mater. Struct. 5 (1998) 10.
[21] T. Obata, K. Komda, T. Nakao, H. Ueba, T. Tasygama, Structural characterization of $Si_{0.7}Ge_{0.3}$ layers grown on Si(001) substrates by molecular beam epitaxy, J. Appl. Phys. 81 (1997) 199.
[22] C. Li, X.C. Li, P.X. Yan, E.M. Chong, Y. Liu, G.H. Yue, X.Y. Fan, Research on the properties of ZnO thin films deposited by using filtered cathodic arc plasma technique on glass substrate under different flow rate of O_2, Appl. Surf. Sci. 253 (1997) 4000.
[23] B. Joseph, P.K. Manoj, V.K. Vaidyan, Studies on preparation and characterization of indium doped zinc oxide films by chemical spray deposition, Bull. Mater. Sci. 28 (2005) 487.
[24] A.M. Sherry, M. Kumar, Analysis of thermal expansion for alkali halide crystals using the isobaric equation of state, J. Phys. Chem. Solids 52 (1991) 1145.
[25] J.L. Tallon, The thermodynamics of elastic deformation—I: equation of state for solids, J. Phys. Chem. Solids 41 (1980) 837.
[26] Q. He, Z.-T. Yan, Study of Temperature Dependence of Bulk Modulus and Interatomic Separation for Ionic Solids, Phys. Status Solidi B 223 (2001) 767.
[27] Y. Al-Douri, H. Abid, H. Aourag, Correlation between the bulk modulus and the charge density in semiconductors, Physica B 305 (2001) 186.
[28] Y. Al-Douri, H. Abid, H. Aourag, Calculation of bulk moduli of semiconductor compounds, Physica B 322 (2002) 179.
[29] (a) Y. Al-Douri, The pressure effect of the bulk modulus seen by the charge density in CdX compounds, Mater. Chem. Phys 78 (2003) 625;
(b) Y. Al-Douri, The pressure effect of the bulk modulus seen by the charge density in CdX compounds, Mater. Chem. Phys. 82 (2003) 499.
[30] J.C. Phillips, Bonds and Bands in Semiconductors, Academic Press, San Diego, 1973.
[31] W.A. Harison, Electronic Structure and the Properties of Solids, General Publishing Company, Toronto, 1989.
[32] M.L. Cohen, Calculation of bulk moduli of diamond and zinc-blende solids, Phys. Rev. B 32 (1985) 7988.
[33] P.K. Lam, M.L. Cohen, G. Martinez, Analytic relation between bulk moduli and lattice constants, Phys. Rev. B 35 (1987) 9190.
[34] Y. Al-Douri, H. Abid, H. Aourag, Empirical formula relating the bulk modulus to the lattice constant in tetrahedral semiconductors, Mater. Chem. Phys. 87 (2004) 14.
[35] Z. Charifi, H. Baaziz, A.H. Reshak, Ab-initio investigation of structural, electronic and optical properties for three phases of ZnO compound, Phys. Status Solidi B 244 (2007) 3154.
[36] H. Karzel, W. Potzel, M. Kofferlein, W. Schiessl, M. Steiner, U. Hiller, G.M. Kalvius, D.W. Mitchell, T.P. Das, P. Blaha, K. Schwarz, M.P. Pasternak, Lattice dynamics and hyperfine interactions in ZnO and ZnSe at high external pressures, Phys. Rev. B 53 (1996) 11425.